JOURNAL OF MAGNETIC RESONANCE **131,** 139–143 (1998)
ARTICLE NO. MN971353

# COMMUNICATIONS

# Localized Eddy Current Compensation Using Quantitative Field Mapping

M. Terpstra, P. M. Andersen, and R. Gruetter[1]

*Center for Magnetic Resonance Research, University of Minnesota, 385 East River Road, Minneapolis, Minnesota 55112*

Received January 7, 1997; revised October 29, 1997

**Eddy current effects induced by switched gradients in proximal conducting structures are traditionally reduced by applying preemphasis currents whose amplitudes and decay characteristics must be set to offset the eddy current fields. We present an expeditious, localized, and quantitative method for mapping and adjusting the parameters for eddy current compensation. Mapping is based on analysis of projections as used in the fast automatic shimming technique by mapping along projections (FASTMAP). Adjustment methods are demonstrated in high-field horizontal bore systems. The proposed localized eddy current mapping technique may also be used for localized measurements in situations where asymmetric conducting structures may cause nonlinear eddy current fields, such as in interventional MRI and open magnet designs.** 

*Key Words:* **eddy currents; rat brain**; *in vivo,* **$^1$H NMR.**

Switched gradients induce eddy currents in nearby conducting structures (*1*), potentially causing image artifacts, localization errors, and signal distortions. Active shielding of gradients reduces eddy currents substantially (*2–5*), yet residual eddy currents may require further reduction. This is commonly achieved by applying preemphasis currents in the appropriate gradient coil and in the homogeneous $B_0$ shim coil (*6–8*). The net effect of this compensatory current is to overshoot the nominal gradient pulse. We describe and illustrate a *localized* eddy current measurement method which is quantitative and provides the basis for an expeditious and versatile compensation. Additionally, the method permits time-resolved analysis of eddy currents generated by any sequence of gradients as a function of time.

Setting of the multiexponential amplitudes and time constants for preemphasis currents traditionally relies upon one or more of the following measurement methods: output of a pick up coil, which requires special hardware and repeated repositioning of the pick up coil (*9, 10*); measuring multiple FIDs of an extended sample after a gradient is turned off, which requires careful sample positioning (*11*); or measurement of small samples at multiple locations in the magnet, which can be a time-consuming procedure due to the requirement that the samples be repositioned repeatedly in the bore (*12, 13*). Another elegant, yet time-consuming semi-quantitative method to image the spatial distribution of eddy current fields has been proposed (*8*). In practice, compensatory currents are determined by iteratively adjusting current values and time constants until eddy current effects are minimized. Such an iterative process is generally neither quantitative, efficient, nor reliable. Our goal was to provide an eddy current compensation procedure based on quantitative spatial measurement of eddy current fields and subsequent noniterative adjustment.

We applied the stimulated echo sequence shown in Fig. 1A to measure eddy current effects after gradient switching. The excitation and refocusing portion of the sequence was based on standard stimulated echo (STEAM) imaging (*14*), applied without slice selection for the first RF pulse and without any phase encoding gradients. The slice-selective (second and third) pulses were applied in the presence of two orthogonal slice gradients similar to the FASTMAP scheme (*15*). The orientation of these slice gradients ($G_{\text{slice1}}$, $G_{\text{slice2}}$) and the corresponding frequency of the pulses ($f_{\text{slice1}}$, $f_{\text{slice2}}$) selected coherences along a bar at an operator-specified, computer-controlled location as indicated in Fig. 1B. The test gradient, labeled $G_{\text{test}}$ in Fig. 1A, generated the eddy currents to be evaluated. To minimize confounding effects from the rising edge of the test gradient, the duration of $G_{\text{test}}$ was set to $\tau = 0.5–1.0$ s. The read gradient ($G_{\text{read}}$) was orthogonal to both slice gradients and thus applied along the bar. Eddy currents generated by the falling edge of $G_{\text{test}}$, whose orientation was set to that of $G_{\text{read}}$, caused additional phase shifts along $G_{\text{read}}$, since the phase of the magnetization during the stimulated echo depended on the average eddy current field generated by $G_{\text{test}}$ during TE1 which was set to 2 or 3 ms. A long TM of 1 s was used to minimize eddy

[1] To whom correspondence should be addressed. Fax: (612) 626-7005. E-mail: gruetter@geronimo.drad.umn.edu.



1090-7807/98 $25.00

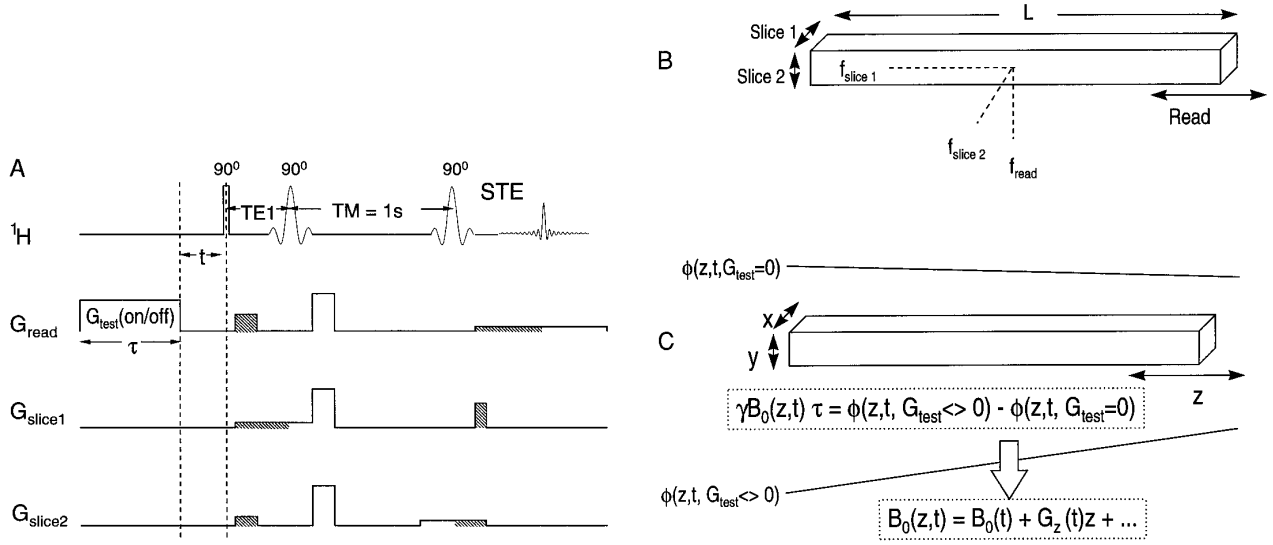


**FIG. 1.** Quantitative and simultaneous measurement of $B_0$ and $G$ generated by $G_{test}$ at time $t$. (A) shows the STEAM-based pulse sequence which was used as in FASTMAP for localization to a thin bar (*15*). The second and third RF pulses select a slab along $G_{read}$. The three gradient axes are orthogonal and $G_{read}$ is permutated through all three magnet axes. The falling edge of $G_{test}$ ($\tau > 0.5$ s) encodes the phase of the echo during TE1. The long TM = 1 s ensures that eddy current effects are negligible in the refocusing period (STE). Shaded areas indicate equal gradient areas needed to refocus magnetization. During TM, a strong crusher gradient applied on all axes eliminated unwanted transverse coherences. (B) illustrates the use of the gradients and corresponding frequencies to localize magnetization along a bar. The dimension along $G_{read}$ is controlled by limiting the range of data analysis along the projection to $\pm L/2$. (C) shows an example along the magnet axis *z*. The phase difference generates a pure eddy current profile along *z* and eliminates phase effects generated by eddy current effects inherent to the proposed localization sequence.

current effects of $G_{test}$ during the stimulated echo refocusing time period (denoted STE in Fig. 1A). To minimize signal loss during the long TM of 1 s we used spherical or cylindrical phantoms filled with distilled or tap water to provide sufficiently long $T_1$. To remove the effect of eddy current fields generated by the STEAM localization, two measurements were acquired sequentially. The first was made with the STEAM sequence as described above. The second was identical except $G_{test}$ was set to zero. Phases generated by the sequence in Fig. 1A with $G_{test} = 0$ were subtracted from phases generated with $G_{test} \neq 0$ by complex division of respective projections (*15*), leaving only phases generated by $G_{test}$, as indicated schematically in Fig. 1C.

Phases calculated within an operator-defined area of interest along the projection generated by $G_{read}$ were used to calculate a constant field term, $B_0(t)$, and a linear term, $G(t)$, along the bar (denoted by the spatial variable $r$) according to

$$\frac{\Delta\phi(r)}{\text{TE1}} = \gamma B_{\text{eddy}}(r, t) = \gamma[B_0(t)] + \gamma[G(t)]r. \quad [1]$$

Eddy currents were determined from the aforementioned analysis along projections by repeating the experiment along each of the three magnet axes for a given recovery time ($t$ in Fig. 1A). The eddy current decay curve was obtained by subsequently increasing $t$ and repeating the experiment. The results of the analysis were stored on disk as $t$ was changed in progressively larger increments from 500 $\mu$s to 1.5 s in at least 20 steps. The process of data gathering along all three magnet axes with a TR of 4 s thus required less than 10 min. To correct for the discontinuity of the arctan function, distortions in the measured $B_0$ drifts were corrected by subtracting a constant equal to $2n\pi$/TE1 after the decay curve had been recorded. Uncompensated $B_0(t)$ and $G(t)$ curves were determined for all three orientations ($G_{read}$ along *x*, *y*, and *z*) in a 9.4-T, 31-cm bore magnet equipped with an 11-cm i.d. actively shielded gradient (Magnex, UK) as well as a 4-T, 125-cm bore magnet (Siemens, Erlangen, Germany and Varian, Palo Alto, CA) equipped with a shielded body gradient (Siemens AS25) upon which we wound a homogenous $B_0$ coil. Uncompensated $B_0(t)$ and $G(t)$ were fitted to the following exponential models using Marquardts compromise method (*16*) and RS1 software (BBN Domain Corporation, Cambridge, MA):

$$B_0(t) = \sum_{j=1}^{n} B_{0_j} e^{-t/t_j} \text{ and } G(t) = \sum_{i=1}^{n} G_i e^{-t/\tau_i}. \quad [2]$$

To determine the best fit for the 9.4-T system, $n$ was increased until the root mean square deviation (RMSD) of $B_0$ was less than 6 Hz and the RMSD of $G < 9$ Hz/cm. On the 4-T system, the criteria for convergence were the RMSD of $B_0 < 1$ Hz and the RMSD of $G < 0.5$ Hz/cm.

Preemphasis time constants ($\tau$) were entered quantitatively into the eddy current compensation unit based on manufacturers specifications. A gradient management unit (Magnex, Abingdon, UK) was used for the 9.4-T system (*17*). The 4-T eddy current compensation unit was a standard Magnetom design (Siemens, Erlangen, Germany), whose potentiometer sensitivity had been reduced approximately fourfold. Both units provided three time constants per axis. The 4-T magnet required only one or two time constants for $B_0$ compensation. The method has also been successfully used in an unshielded 33-cm head gradient in the 4-T system, in an actively shielded 25-cmi.d. gradient coil in the 9.4-T system, and in a 25-cm gradient coil placed in a 40-cm bore, 5-T system (not shown).

Amplitude ($B_{0j}$ and $G_i$) settings in both compensation units were not quantitative. This was not detrimental to the adjustment procedure since the potentiometer settings were determined empirically according to the following procedure:

(i) For each orientation the longest time constant, $\tau_n$ (Eq. [2]), was entered into the unit while the corresponding potentiometer setting for the corresponding amplitude (preemphasis $G_i$) was estimated.

(ii) Using the sequence in Fig. 1 the residual $G(t)$ was measured at a relatively long time $t$ compared to $\tau_i$, where the effects of all shorter $\tau_i$ components ($\tau_i < \tau_n$) were negligible. Typically $t$ was set to be three times the next longest $\tau_i$.

(iii) The preemphasis $G_i$ entered in the compensation unit was adjusted iteratively until the remaining measured $G(t)$ was minimized.

Steps (i–iii) were then repeated for the progressively smaller $\tau_i$ at decreasing $t$ while leaving the longer $\tau_i$ and $G_i$ at their previously determined level. After minimizing $G(t)$, $B_0(t)$ was adjusted in a completely analogous fashion. Adjustment of the amplitudes required at most 2 min per time constant, thus providing an adjustment time of less than 1 h. With an ideal transfer function and quantitative, calibrated amplitudes this time should be reduced to the time needed to enter the correction terms, i.e., a few minutes.

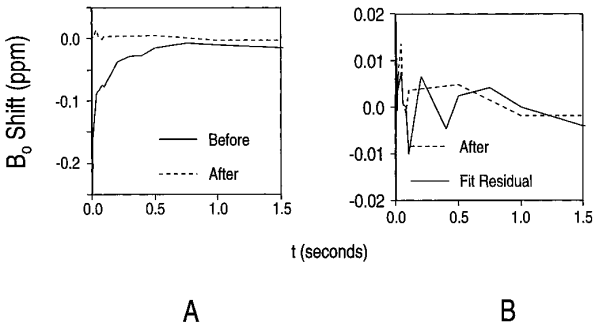


**FIG. 2.** (A) $B_0(t)$ shift generated by a 1.0-s $G_{test}$ of 14 mT/m along $z$ before and after compensation. (B) Expanded, compensated $B_0(t)$ shift and the fit residual, i.e., uncompensated data minus the $B_0$ fit of Eq. [2]. Data were acquired on a 4-T, 125-cm bore magnet (Siemens/SISCO) equipped with a shielded whole-body gradient (Siemens Vision).

To verify proper operation of the adjustment procedure, the residual $B_0(t)$ and $G(t)$ were measured using the sequence in Fig. 1 after optimizing preemphasis for $B_0$ and $G$ in all three directions. Figure 2A represents $B_0(t)$ generated by a 1.0-s long 14 mT/m $G_{test}$ along $z$ measured in the 4-T magnet with shielded whole-body gradient before (solid curve) and after (dotted curve) eddy current compensation was performed as described above. The largest $B_0$ shift before compensation was $-0.24$ ppm ($-41$ Hz), and a $B_0$ field shift larger than $-0.02$ ppm ($-3.4$ Hz) persisted as long as 0.5 s. Compensation reduced the $B_0$ shift by at least 10-fold. At times greater than 0.2 s, $|B_0 \text{ shift}| < 0.005$ ppm (0.85 Hz). At all times $|B_0|$ was reduced below 0.014 ppm (2.4 Hz). Figure 2B shows the remaining $B_0(t)$ after compensation (dotted curve) at an expanded vertical scale and compares it to the residual of the fit to the uncompensated data (solid curve), i.e., the uncompensated data minus the $B_0$ fit of Eq. [2]. Compensated data compare well to the fit residual in magnitude and time variation. Typical linewidths at 4 T were 5–8 Hz for metabolites and 7–9 Hz for water. After compensation, lineshapes and water suppression were substantially improved; thus resonances close to the water could be routinely observed (*18*).

The $G(t)$ generated by a 1.0-s-long 92 mT/m $G_{test}$ along $z$ (9.4-T, 33-cm bore magnet, 11-cm actively shielded gradient) before (solid line) and after (dotted line) eddy current compensation is shown in Fig. 3A. Before compensation the largest gradient along $z$ was $-0.35\%$ ($-137$ Hz/cm) and a gradient larger than $-0.025\%$ ($-10$ Hz/cm) persisted as long as 0.5 s. Compensation substantially reduced the gradient to less than 0.01% (4 Hz/cm) at 200 ms or longer and to less than 0.02% (8 Hz/cm) at all times. Figure 3B is a vertically expanded plot of the compensated data (dotted line) compared to the residual of the fit to the uncompensated data (solid line). Compensated data follow the fit residual very closely in terms of both magnitude and time variation.

Most pulse sequences use short gradient pulses, where the rising edge partially compensates eddy currents generated by the falling edge. We found that even when using short gradient pulses and actively shielded gradients, preemphasis was necessary to attain optimal quality. Neither phase distortions nor excess line broadening were generated in the presence of preemphasis correction, eliminating the need for post processing correction methods (*19–21*). Typical linewidths at 9.4 T were 6–12 Hz for metabolites and 11–18 Hz for water. After compensation, lineshapes and water suppression were substantially reduced with the current method as illustrated by the excellent quality of $^1$H NMR spectra in rat brain (Fig. 4), which is consistent with results achieved in dog brain at 9.4 T (*22, 23*). The excellent performance of

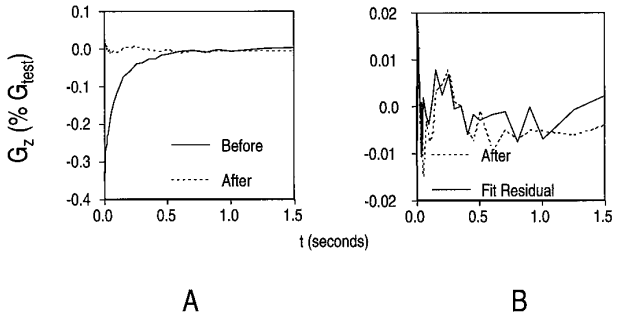


**FIG. 3.** (A) $G(t)$ generated by a 1.0-s $G_{test}$ of 92 mT/m along $z$ before and after compensation. (B) Expanded, compensated $G(t)$ and the fit residual. Data were acquired on a 9.4-T, 33-cm bore magnet equipped with an 11-cm actively shielded gradient (Magnex, UK).

**TABLE 1**

**$B_0$ Field Shifts and Gradients Generated by a 92 mT/m $G_{test}$ (1.0 s Duration) before and after Application of Eddy Current Compensation on the 9.4-T System**

| Eddy current component | \|Maximum value\| before compensation | \|Maximum value\| after compensation |
|---|---|---|
| $B_{0x}$ (Hz) | 96 | 10 |
| $G_x$ (Hz/cm) | 117 | 9 |
| $B_{0y}$ (Hz) | 43 | 3 |
| $G_y$ (Hz/cm) | 168 | 10 |
| $B_{0z}$ (Hz) | 202 | 16 |
| $G_z$ (Hz/cm) | 137 | 8 |

the eddy current compensation can be judged from the fact that shimming was achieved by FASTMAP (*15*), a shim method that provides optimal results when data acquisition with the actual localization sequence is not influenced by eddy current effects.

For both 4-T and 9.4-T configurations, $B_0$ and $G$ in all three orientations were reduced by at least 10-fold. Values before and after compensation for the 9.4-T configuration are provided in Table 1. Generally, the $B_0(t)$ and $G(t)$ remaining after compensation closely followed the residual of the fit, indicating that only nonmodeled components of $B_0$ and $G$ remained, which further illustrates the precision of the methodology. The accuracy of the compensation method was illustrated by its ability to remove eddy current effects to a negligible level.

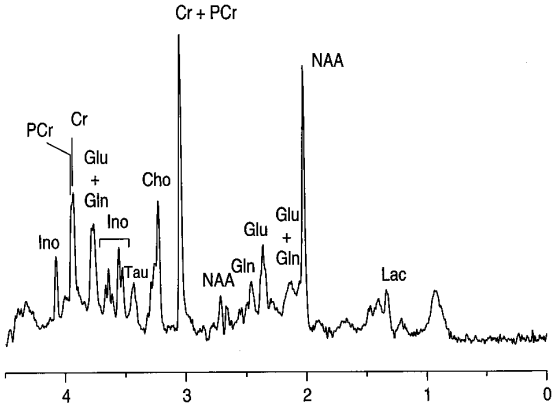


**FIG. 4.** Example of spectral quality achievable *in vivo* using the present eddy current compensation method. Shown is a $^1$H NMR spectrum of a 64-$\mu$l volume in rat brain obtained using 3,1-DRY-STEAM at 9.4-T, implemented as described previously (*18*). Water suppression was achieved with 15-ms Gaussian pulses. The spectrum was zero-filled eight times prior to Fourier transformation, was processed with 3-Hz Lorentz-to-Gauss apodization, and is shown without any baseline correction or filtering. Shimming was performed using FASTMAP (*15*). Linewidths were approximately 10 Hz for the metabolites and 12 Hz for water.

It should be emphasized that the $B_0(t)$ and $G(t)$ generated by any sequence of gradients can be characterized using the sequence shown in Fig. 1A. For example, settling time can be chosen based on field homogeneity requirements or limitations *in vivo*. Based on the reasonable requirement that distortions generated by eddy currents do not spread spectral intensity outside the peak of interest, convergence criteria such as

$$|\gamma B_0| \leq \frac{\Delta\nu_{1/2}}{4} \text{ and } |\gamma G| \leq \frac{\Delta\nu_{1/2}}{4a} \qquad [3]$$

may be set where $\Delta\nu_{1/2}$ is the linewidth of the peak of interest, and $a$ is the approximate dimension of the localized volume. Under these criteria, the $B_0$ shift generated by eddy currents induces a frequency shift less than one-fourth of the best linewidth and the gradient generated by eddy currents induces line broadening less than one-fourth of the linewidth achieved over the localization volume specified. For the 9.4-T system used here and the 12-Hz linewidth observed in a 64 mm$^3$ volume (Fig. 4) these criteria require that after a given localization sequence $\gamma B_0$ be below 3 Hz and $\gamma G$ be below 8 Hz/cm. In the 4-T system (6 Hz linewidth and 27 cm$^3$ volume) these criteria require a maximal $B_0$ of 1.5 Hz and a maximal eddy current of 0.7 Hz/cm.

We have used the magnet isocenter to determine optimal gradient compensation settings. However, the present scheme can easily be modified to provide a localized measurement by suitable selection of the frequencies ($f_{slice1}$, $f_{slice2}$) applied for the second and third pulses in Fig. 1. Such localized measurements of eddy current effects may be necessary whenever asymmetric conducting structures such as RF shields in RF coils or interventional devices are brought into the gradient coil close to the sample or in open magnets.

Eddy current compensation on the 9.4-T gradient insert was less efficient than on the 4-T gradient coil. This can be explained by the much closer proximity of the heat shield in the 9.4-T system. It also reflects the fact that correction

is more stringent when measuring bigger volumes from narrower peaks as was the case at 4 T.

The eddy current mapping method described is quantitative, localized, accurate, versatile, and expeditious. Provided that preemphasis amplitudes can be specified quantitatively in the eddy current compensation hardware, the compensation method is completely quantitative, facilitating a singular hardware adjustment. Because the method is localized, neither multiple samples nor precise sample positioning are necessary in contrast to most other techniques. Our practice from several systems suggested that one order of magnitude reduction in eddy currents is feasible. If more reduction is required, increased distance to the heat shield may be necessary. We conclude that eddy current effects can be efficiently compensated at high fields to a level allowing high-resolution $^{1}$H NMR with very short echo times. In addition, eddy currents generated by any sequence of gradients as a function of time can be analyzed efficiently and accurately.

## ACKNOWLEDGMENTS

The authors thank Dr. Michael Garwood for support and encouragement and Dr. Hellmut Merkle for maintenance and improvement of the spectrometer hardware. This work was also supported by NIH (RR08079 and CA64338) and the W. M. Keck foundation.

## REFERENCES

1. S. R. Thomas, ''The Physics of MRI'' (M. J. Bronskill and P. Sprawls, Eds.), p. 90, American Institute of Physics, Woodbury, NY (1993).
2. P. Mansfield and B. Chapman, *J. Magn. Reson.* **66,** 573 (1986).
3. R. Turner, *J. Phys. E* **21,** 948 (1988).
4. R. Bowtell and P. Mansfield, *Meas. Sci. Technol.* **1,** 431 (1990).
5. C. D. Eccles, S. Crozier, W. Roffman, D. M. Doddrell, P. Back, and P. T. Callaghan, *Magn. Reson. Imaging* **12,** 621 (1994).
6. P. Jehenson, M. Westphal, and N. Schuff, *J. Magn. Reson.* **90,** 264 (1990).
7. J. J. Van Vaals and A. H. Bergman, *J. Magn. Reson.* **90,** 52 (1990).
8. C. H. Boesch, R. Gruetter, and E. Martin, *Magn. Reson. Med.* **20,** 268 (1991).
9. J. Chankji, J. L. Lefevre, and A. Briguet, *J. Phys. E* **18,** 1014 (1985).
10. D. J. Jensen, W. W. Brey, J. L. Delayre, and P. A. Narayana, *Med. Phys.* **14,** 859 (1987).
11. R. E. Wysong and I. J. Lowe, *Magn. Reson. Med.* **29,** 119 (1993).
12. S. Robertson, D. G. Hughes, Q. Liu, and P. S. Allen, *Magn. Reson. Med.* **25,** 158 (1992).
13. Q. Liu, D. G. Hughes, and P. S. Allen, *Magn. Reson. Med.* **31,** 73 (1994).
14. J. Frahm, K. D. Merboldt, W. Hanicke, and A. Haase, *J. Magn. Reson.* **64,** 81 (1985).
15. R. Gruetter, *Magn. Reson. Med.* **29,** 804 (1993).
16. W. H. Press, B. P. Flannery, S. A. Teukolsky, and W. T. Vetterling, ''Numerical Recipes in Pascal,'' p. 572. Cambridge Univ. Press, Cambridge (1989).
17. M. E. Fry, S. Pittard, I. R. Summers, W. Vennart, and F. T. D. Goldie, *J. Magn. Reson. Imaging* **7,** 455 (1997).
18. R. Gruetter, M. Garwood, K. Ugurbil, and E. R. Seaquist, *Magn. Reson. Med.* **36,** 1 (1996).
19. R. J. Ordidge and I. D. Cresshull, *J. Magn. Reson.* **69,** 151 (1986).
20. U. Klose, *Magn. Reson. Med.* **14,** 26 (1990).
21. J. R. Roebuck, D. O. Hearshen, M. O'Donnell, and T. Raidy, *Magn. Reson. Med.* **30,** 277 (1993).
22. R. Gruetter, S. A. Weisdorf, V. Rajanayagan, H. Merkle, C. L. Truwit, F. B. Cerra, and S. L. Nyberg, Abstracts of the Society of International Magnetic Resonance in Medicine, 5th Annual Meeting Vancouver, BC, p. 239 (1997).
23. S. L. Nyberg, F. B. Cerra, R. Gruetter, *Liver Surg. Transpl.* **4,** 1–9 (1998).